WILEY-VCH

A near-infrared probe for detecting and interposing amyloid beta oligomerization in early Alzheimer's disease

Li Quan,[1,2]* Ines Moreno-Gonzalez,[3,6,7]* Zhigang Xie[4]*, Nazaret Gamez,[3,6] Qinyong Song,[1] Jianhua Gu,[5] Laura Vegas-Gomez,[6] Wenhai Lin,[4] Ruben Gomez-Gutierrez,[3] Tianfu Wu,[2]*

[1] Jiangsu Provincial Engineering Research Center for Biomedical Materials and Advanced Medical Devices, Faculty of Mechanical and Material Engineering, Huaiyin Institute of Technology, Huai'an 223003, Jiangsu Province, China.

[2] Department of Biomedical Engineering, University of Houston, Houston, Texas 77204, USA.

[3] The University of Texas Health Science Center at Houston, Houston, Texas 77030, USA.

[4] State Key Laboratory of Polymer Physics and Chemistry, Changchun Institute of Applied Chemistry, Chinese Academy of Sciences, Changchun, 130022, China.

[5] Electron Microscopy Core, Houston Methodist Research Institute, Houston, TX 77030, USA.

[6] Department of Cell Biology, Genetic and Physiology, Faculty of Sciences, Instituto de Investigacion Biomedica de Malaga-IBIMA

[7] Networking Research Center on Neurodegenerative Diseases (CIBERNED), University of Malaga, Malaga, Spain.

Correspondence

Li Quan, E-mail: quanli99@126.com.

Tianfu Wu, E-mail: twu13@central.uh.edu.

Ines Moreno-Gonzalez, Email: inesmoreno@uma.es.

Zhigang Xie, E-mail: xiez@ciac.ac.cn.

KEYWORDS

Alzheimer's disease, Diphenylalanine, BODIPY, β-amyloid oligomer, Near-infrared probe

ABSTRACT

The misfolding and deposition of beta-amyloid (Aβ) in human brain is the main hallmark of Alzheimer's disease (AD) pathology. It is believed that one of the drivers of Alzheimer´s pathogenesis is the production of soluble oligomeric Aβ. Diphenylalanine (FF) at the C-terminus of Aβ fragments plays a key role in inducing the pathology. Based on the hydrophobic structure of FF, we synthesized a near-infrared BF_2-dipyrrolmethane fluorescent imaging probe (NB) to detect both soluble and insoluble Aβ. NB not only binds Aβ but also interposes self-assembly of Aβ through π-π interaction between NB and FF. This work holds great promise in early diagnosis of AD and may also provide an innovative approach to slow down and even halt AD onset and progression.

1 INTRODUCTORY NARRATIVE

1.1 Contextual background

Alzheimer's disease (AD) is a chronic degenerative brain disease, and the increase of one AD patient occurs in every three seconds worldwide, however, the prevention and treatment of this disease are largely unresolved.[1, 2] To date, the only five drugs approved by the US Food and Drug Administration (FDA) to treat AD are all palliative. Unfortunately, these medications are not able to alleviate pathological changes or delay the progression of AD.[3] Importantly, the lack of early and accurate diagnosis of AD and disease surveillance further hinders the development of therapeutic drugs. Although the precise mechanism that triggers AD is unknown, there is a large body of scientific evidence suggesting that β-amyloid (Aβ), particularly soluble aggregated forms, or amyloid oligomers, cause neuronal damage and cell death leading to the disease.[4-8] So far, the detection of Aβ plaques in post mortem brain samples have been the gold standard for clinical diagnosis of AD.[9-12] However, the Aβ plaques are only associated with late-stage AD,[9, 13] and the early diagnosis of AD is still clinically unavailable.

It is known that Aβ monomers assemble into different forms of oligomers, which further aggregate into fibrils.[14] Aβ oligomers induce greater toxicity than other Aβ aggregation, and inhibit neuronal viability 10-fold more than Aβ fibrils and 40-fold more than Aβ monomers.[15] Aβ oligomers include dimers, trimers, tetramers, pentamer and hexamer, among which tetramers have the greatest toxicity damage to human brain and have the strongest correlation with AD in the early stage.[14] Hence, oligomeric Aβ may be a promising early biomarker for AD. Unfortunately, a robust probe to detect oligomeric Aβ is still lacking. Diphenylalanine (FF), as the smallest unit and core recognition motif of Aβ, can self-assemble into nanofibers, which induces early onset of AD.[11, 16] Therefore, it is intriguing to diagnose AD via the detection of the FF motif in Aβ, however, this line of research is largely missing. To fill this knowledge gap, our group identified a boron-dipyrromethene (BODIPY) based probe to detect and drive self-

assembly of FF from a synthetic BODIPY.[17] A green fluorescent BODIPY probe (named "X1") exhibited specific responses to FF nanofibers with strong fluorescence signals. Upon binding to FF, X1's fluorescence intensity was increased by 3.6 fold (△F/F).[17] Based on the structure of X1 probe, we further synthesized a significantly improved novel near-infrared fluorescent probe for the detection of oligomeric Aβ.

1.2. Unique aspects of the probe design and significance of the results

The structure of X1 was modified to obtain a near-infrared BODIPY fluorescence probe (NB) for the purpose of early diagnosis of AD (**Scheme 1A**). The design shown in **Scheme 1B** was based on the fact that the two aromatic rings of FF overlap well with the two aromatic rings of NB to form a stable π-π structure; while the carboxyl and amino groups of FF further promote the NB-FF binding. When Aβ folds and further aggregates into oligomers, NB binds effectively to the exposed FF of Aβ, which leads to the favorable detection of AD through fluorescence imaging. Aβ fibril contains a shallow groove formed by alternating conformers of aromatic rings, stabilized by packing interactions with adjacent residues, which is indispensable for a probe to bind and recognize Aβ fibrils. However, due to a greater steric hindrance, NB was not able to enter the aromatic shallow groove, hence NB could not stain Aβ fibrils. In contrast, in the Aβ oligomers, as a β-folding site as well as a NB binding motif, FF is completely exposed which enables NB to recognize and respond to Aβ oligomers robustly. For free NB, benzene rings of NB rotate freely within certain range (**Scheme 1B**). Its excitation and emission wavelengths in 50% ethanol are 591 nm and 682 nm, respectively (**Figure S1**). When NB binds to Aβ oligomers through π-π/hydrogen interactions between NB and FF, the rotation of the benzene rings is restricted, which enhances the whole co-planarity. As a result, NB fluorescence increases by 1650% after binding to Aβ oligomers (**Scheme 1B**). As is well-known, Aβ derives from the proteolytic cleavage of a larger glycoprotein named amyloid precursor protein (APP) by β- and γ- secretase (**Scheme 1C**).[18, 19] In the starting point of Aβ folding and aggregation,

FF plays a key role.[20] Four β-folded Aβs are organized in a face-to-back assembly to form oligomeric Aβ, which is an important physiological marker in the early stage of AD and harms the brain.[14, 21] When the β-folded Aβ forms tetrameric Aβ oligomers, FFs are almost completely exposed, creating an excellent position for NB's specific binding with FF (**Scheme 1D**), and enabling the early diagnosis of AD via fluorescence imaging.[4, 14] Aβ oligomers increasingly rotate at 90° along the β-folds chain direction to become Aβ fibrils, which are larger Aβ aggregates than octamers and associated with the metaphase/late-stage AD.[14, 22] When β-folded Aβ form fibrils, with hydrophobic fragments (including FF) clustered at the core of the spherical structure, most FFs participate in self-assembly of Aβ and form spherical structures resulting in poor NB binding to Aβ fibrils (**Scheme 1D**).[22] Moreover, Aβ monomers exhibit more free elasticity which may result in poor response of NB to Aβ monomers.[14]

Collectively, NB could effectively differentiate in response to oligomers and monomers/fibrils to serve the purpose of AD early diagnosis. As a potential new near infrared fluorescent probe for imaging AD brain pathology, the benzothiazole structure of NB benefits Aβ binding selectivity, whereas a short distance (11.4 - 16.2 Å) between the benzothiazole-containing donor and acceptor (Figure S3) favors Aβ aggregates.[23] In this study, the NB probe not only exhibited excellent responses in binding oligomeric Aβ and inhibitory effect on Aβ aggregation in *in vitro* experiments, but also successfully detected oligomeric Aβ in AD brain tissue using confocal microscopy. However, whether NB is a viable probe for *in vivo* imaging of oligomeric Aβ in AD brain is unanswered in this study. Therefore, to assess the performance of NB in preclinical studies and to determine the functionality of NB in reflecting disease stages are recommended in future studies.

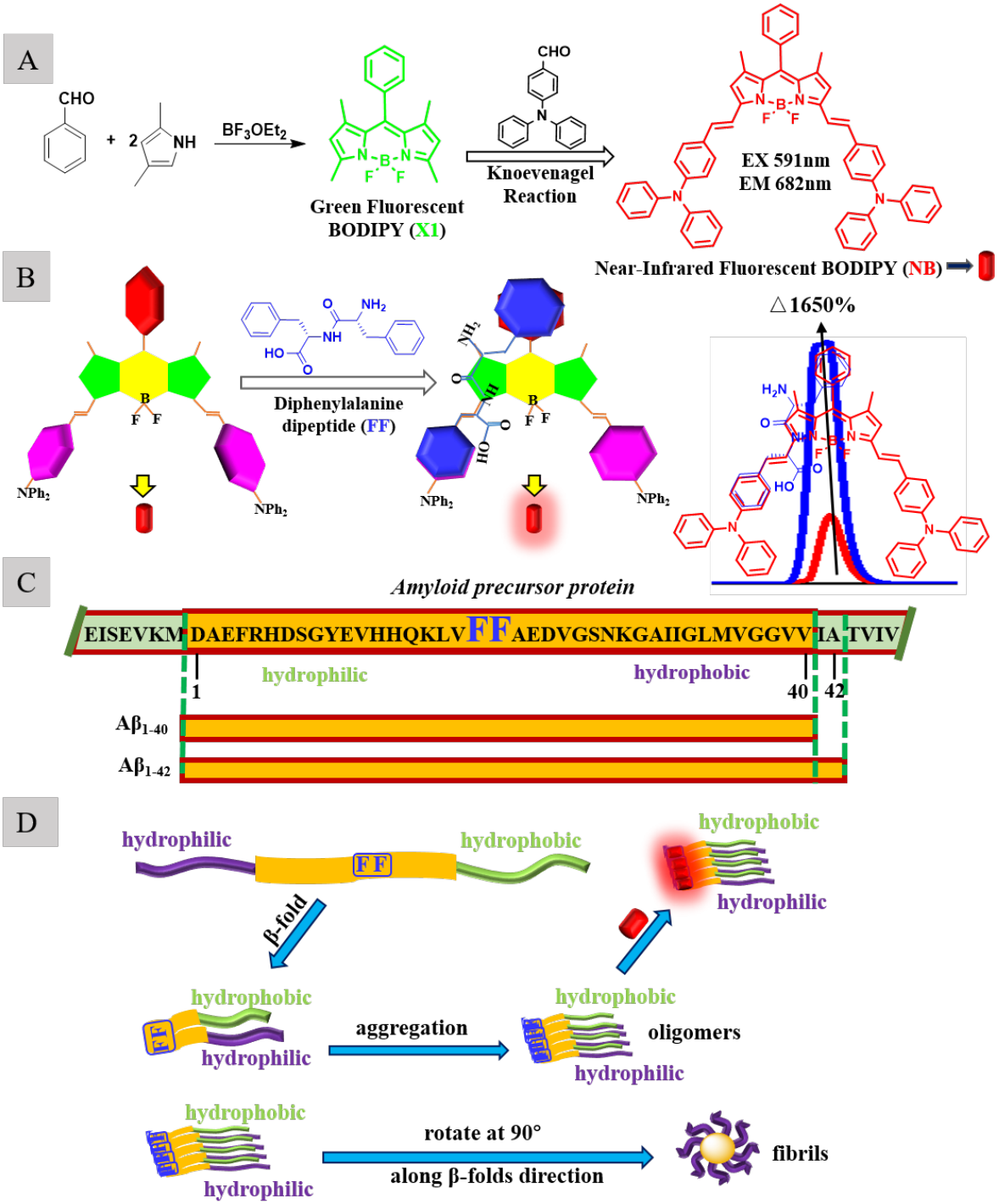

Scheme 1. Aβ derives from the proteolytic cleavage of a larger glycoprotein named amyloid precursor protein.[18] (A) A near-infrared BODIPY probe (NB) was synthesized by structural modification of an analog of X1 which detected and drove self-assembly of FF.[17] (B) NB was designed according to the structure of FF and the two aromatic rings of FF overlap well with the two aromatic rings of NB. When NB binds to Aβ oligomers, free rotation of the three benzene rings of NB is restricted resulting in 1650% increasing of NB fluorescence. (C) Overview of the amino acid sequences of the Aβ-related peptides $A\beta_{1-40}$ and $A\beta_{1-42}$. (D) Aβ produces β-folds and then aggregates to form tetrad oligomers. NB could be potentially useful in the early diagnosis (via imaging) of AD via binding to the FF of oligomeric Aβ. On the other hand, the tetramer could rotate 90° along the β-fold axis to form fibrils.

3. DETAILED METHODS AND RESULTS

3.1. Methods

3.1.1 Measurement and instrument

Electron microscopy imaging were obtained from Atomic Force Microscopy (AFM)/Scanning Electron Microscopy (SEM) Core of Houston Methodist Hospital Research Institute. All starting materials were purchased from Sigma-Aldrich and Fisher Scientific Worldwide Inc, unless otherwise noted. ^{1}H-NMR spectra were recorded on a Bruker NMR 400 DRX Spectrometer at 400 MHz and referenced to the proton resonance resulting from deuterium generation reagent. The mass spectra of samples were recorded using a Thermo LTQ-Orbitrap XL ETD TOF mass spectrometer. Fluorescence experiments were performed using Perkin ElmerLS-55 Spectrofluorophotometer and Hitachi Fluorescence spectrophotometer F-7000. Nava Nano SEM 230 (FEI) was used for SEM analysis. All tests were in room temperature and under vacuum (2E-6 Torr). 50μl of sample solution was dropped onto silicon wafer, and the sample was left dry in ambient condition for overnight. The samples were coated with a thin Ir (iridium) film (7nm in thickness) with a sputter Coater (208HR High Resolution Sputter Coater, Ted Pella Inc.) The confocal images were obtained using a Nikon C2+ laser-scanning confocal microscope (Nikon, Tokyo, Japan) and an Olympus FV3000 Confocal Imaging System (Olympus, Tokyo, Japan). Atomic force microscopy (AFM) multimode 8 with a top-mounted optical microscopes was used to attach 5μm micro particles on AFM cantilevers by silicon glue to measure intermolecular forces between probe NB and FF nanofibers or Aβ oligomers. MLCT and NP-O10 AFM cantilevers (Bruker) were used with average spring constant at 0.01N/m and 0.06N/m, respectively. FF was grown on mica. Force curves were acquired with contact mode with a set-point force is about 1nN. Both spring constant and sensitivity of the probe were calibrated under thermal tune condition with the controlling software. Force curves were interpreted with a data analysis software NanoScope Analysis 1.40 (Bruker).

3.1.2 Synthesis of NB probe

To a mixture of aldehyde compound (10 mmol) and 2,4-dimethypyrrole (20 mmol) in CH_2Cl_2 (500 mL), trifluoroacetic acid (2.47 mmol) was added under nitrogen. The reaction mixture was stirred for 4h at room temperature, then 2,3-dichloro-5,6-dicyano-1,4-benzoquinone (DDQ, 10 mmol) in the mixed solvents of CH_2Cl_2 (25 mL) and tetrahydrofuran (25 mL) was added and stirred for 1h. Then Et_3N (12 mL) and BF_3•Et_2O (12 mL) were added dropwise under ice-cold conditions. The mixture was stirred for 30 min before warming up to room temperature, and was stirred for additional 3h at room temperature. The reaction mixture was washed with water (200 mL) for three times, and the organic layers were combined and dried over anhydrous $MgSO_4$. The solvent was evaporated in vacuum, and the residue was purified by column chromatography (Silica gel, eluent: CH_2Cl_2) to obtain powder. The target product was confirmed by NMR and MS. Compound X1: ^{1}H NMR (300 MHz, DMSO-D_6): δ = 1.95 (s, 6H), 2.29 (s, 6H), 5.98 (s, 2H), 7.31-7.37 (m, 5 H); TOF MS EI+ (nature of the peak) calculated: 324.2, observed: 324.3. The green fluorescent X1 was further modified by aldehyde compound. Specific steps are as follows: green fluorescent X1 (0.54 mmol), aldehyde compound (4-(diphenylamino)benzaldehyde, 0.54 mmol, 1 equiv or 1.08 mmol, 2 equiv), and p-toluenesulfonamide (PTSA) (0.01 mmol) were dissolved in toluene (25 mL) and piperidine (1 mL) in a round-bottom flask equipped with a Dean−Stark apparatus. The resulting solution was heated at 140 °C until all solvents were collected by the Dean−Stark apparatus. Toluene (25 mL) and piperidine (1 mL) were added to the solid reaction media and the drying protocol was repeated four times. The resultant materials were then purified by chromatography on silica gel (1:3 dichloromethane/petroleum ether) to obtain dark solid product. The target product NB was confirmed by NMR and MS. ^{1}H NMR (300 MHz, DMSO-D_6): δ = 7.77 (d, J = 4.1 Hz, 4H), 7.24-7.34 (m, 13H), 7.13-6.95 (m, 18H), 6.79 (d, J = 8.2 Hz, 1 H), 6.02 (s, 1H), 5.67 (d, J = 8.2 Hz, 1 H), 2.29 (s, 3H), 1.95 (s, 3H); TOF MS EI+ (nature of the peak): 834.37 (calculated)/ 834.4 (observed).

3.1.3 Self-assembly of FF and BODIPY-labelled FF

NB and FF were dissolved in 45 μL of 1,1,3,3,6,6-hexafluoro-2-propanol (HFP), and then 105 μL of water was added into the solution, followed by ultrasonic treatment at room temperature for 5 ~ 10 min. When the HFP was completely evaporated, FF self-assembly in water was kept in dark place at 4℃ until use.

3.1.4 Production and purification of amyloid beta 40 ($A\beta_{40}$)

E. coli cells (BL21 (DE3) pLysS Competent Cells) harboring pET28 GroES-Ub-Aβ40 plasmid were grown in Luria broth (LB) supplemented with Kanamycin (50 μg/mL) at 37℃, and the expression was induced with 0.4 mM IPTG. After 6 hours of culture, the cells were harvested and lysed with a lysis buffer (50 mM Tris-HCl, pH 8.0, 150 mM NaCl, 5 mM EDTA, 0.5% triton X-100, 1mM DTT and 0.1 mM PMSF). After 30 min on ice, lysozyme (1 mg/mL) was added to the resuspended pellet and incubated for 20 min at RT. Then the resuspended pellet was sonicated and centrifuged at 15,000 x g for 30 min. The resultant pellet was resuspended in lysis buffer, sonicated and centrifuged twice. After 4 washing steps, 3 steps with washing buffer I (50 mM Tris-HCl, pH 8.0, 150 mM NaCl, 5 mM EDTA, 0.5% triton X-100 and 1mM DTT) and the last washing step with washing buffer II (50 mM Tris-HCl, pH 8.0, 150 mM NaCl, 5 mM EDTA and 1mM DTT), inclusion bodies were obtained by centrifugation at 15,000 x g for 30 min. The inclusion bodies were resuspended in a solubilization buffer (50 mM Tris-HCl, pH 8.0, 150 mM NaCl, 1 mM DTT and 8 M urea). The insoluble proteins were removed by centrifugation at 30,000 x g for 30 min. The supernatant containing GroES-Ub-$A\beta_{40}$ fusion protein was collected and purified through a Ni-NTA column. To cleave off $A\beta_{40}$ from the fusion protein, the latter was diluted 3-fold with resuspension buffer (50 mM Tris-HCl, pH 8.0, 150 mM NaCl and 3 M urea) and digested with recombinant a de-ubiquinating enzyme (Usp2cc), 1:100 enzyme to substrate molar ratio at 37℃ for 2 h. After digestion, the samples were sonicated and centrifuged at 30,000 x g for 30 min. The supernatant was loaded on a PRP-

3 Reversed-Phase column (21.5 mm×250 mm, Hamilton Company, USA) for purification of $A\beta_{40}$ with a solvent system buffer 1 (10 mM ammonium acetate, pH 10, 2% acetonitrile) and buffer 2 (70% acetonitrile) at a flow rate of 10 ml/min using a 0-20% linear gradient of buffer 2 for 5 min, then the 20%-40% linear gradient for 30 min and finally 40%-100% for 30 min. The purified $A\beta_{40}$ was lyophilized and stored at −80℃ until use.

3.1.5 Preparation of aggregate-free $A\beta_{40}$

The lyophilized $A\beta_{40}$ was dissolved in 500 μL of 0.1% Ammonium Hydroxide (NH_4OH) to make 1 mg/mL and filtered through a 30 kDa cutoff filter (Amicon Ultra Centrifugal Filter Units, Millipore, Cat No: UFC503096) at 14,000 x g for 12 min to remove large aggregates. The protein concentration was measured by a Micro BCA™ Protein Assay Kit (Pierce, Cat No: 23235) and stored at −80℃ until use.

3.1.6 Preparation of Aβ oligomers

$A\beta_{40}$ oligomers were prepared as described previously.[24, 25] $A\beta_{40}$ peptide (Chinapeptides, Shanghai, China) was dissolved in 100% hexafluoroisopropanol to 1 mM, and then the hexafluoroisopropanol was removed by vacuum. The peptide was resuspended in dimethyl sulfoxide to 5 mM and further diluted by F12 (without phenol red) culture medium to 100 mM and incubated for 24 hours at 4℃. The solution was centrifuged at 14,000 g for 15 min, and the supernatants were collected for use or stored at -20℃.

3.1.7 Measurement of the constant for binding of Aβ oligomers in vitro

A mixture (100 μL of 50% EtOH) containing NB (0−100 nM) and $A\beta_{40}$ oligomers (2 μM) was incubated at room temperature for 30 min. Fluorescence intensity at 682 nm was recorded. The K_d and B_{max} binding curve was generated using GraphPad Prism 5.

3.1.8 In vitro Aβ aggregation assay

NB was first tested as a fluorescence probes for $A\beta_{40}$ in an *in vitro* aggregation assay. Briefly, the purified, aggregate-free $A\beta_{40}$ (2 μM) was incubated in 100 mM Tris-HCl buffer, pH 7.4 at 20°C in opaque 96-well plates with cycles of 1-minute cyclic agitation (500 rpm) every 30 minutes. The aggregation was monitored by adding either Thioflavin T (ThT) or NB to the wells containing aggregate-free $A\beta_{40}$ at the beginning of the reaction. Probes were previously diluted in 50% ethanol and added to the wells to a final concentration of 5%. The fluorescence emission was measured at 485 nm after excitation at 435 nm for ThT, or at 682 nm after excitation at 591 nm for NB using a plate reader (SpectraMax® iD3 Multi-Mode Microplate Reader, Molecular Devices, USA) and the data was fitted using Boltzmann equation. The normalized fluorescence intensity was calculated using the highest fluorescence value as 100% and all data were calculated proportionally to the highest fluorescence. All calculations and graphs were performed using GraphPad Prism 5.

3.1.9 Histological analysis

Mouse samples. Brain tissue from adult 9 month-old APPswe/PS1dE9 AD mouse model (both male and female) was used for histological analysis. Wild-type littermates were used as negative controls. Paraffin-embedded tissue was sliced in sagittal sections of 10μm thick, 3-4 slices were used per mouse. For double staining, sections were incubated overnight with the following primary antibodies: OC rabbit polyclonal antibody (1:1000, Sigma-Aldrich) and A11 rabbit polyclonal antibody (1:1000, EMD Millipore). Then, the tissue was incubated with NB (100μM) in 50% EtOH. For double staining with Thioflavin S (ThS), brain sections were incubated for 5 minutes in 0.025% ThS in 50% ethanol, washed and stained with NB (100μM) in 50% ethanol. Finally, all sections were rinsed and covered using FluorSave Reagent (Merck Millipore) for histological evaluation under an epifluorescence microscope and confocal laser microscope (Nikon A1R).

Human samples. Paraffin-embedded AD patient brain (Braak VI; female; age 76 years) was sliced in 10μm sections and treated with an autofluorescence eliminator reagent (Millipore). Then, sections were heated to 80 ° C for 30 min in 10 mM citrate buffer at pH 6. Samples were incubated with NB (50μM) in 100% ethanol for 8 minutes, followed by incubation with primary antibodies: OC rabbit polyclonal antibody (1:2000, Sigma-Aldrich) overnight, and A11 rabbit polyclonal antibody (1:500, EMD Millipore) for 48h. As a negative control, no NB or primary antibody was used. For ThS/NB staining, brain sections were incubated for 5 minutes in 0.025% ThS (50% ethanol), washed, and incubated with NB (100% ethanol). After rinsing, samples were covered with an antifade mounting medium with DAPI (Vectashield). Microscopy images were taken using the 40x objective lens in a Leica SP8 confocal laser microscope.

3.2. Results

FF is a key recognition motif for Aβ peptide to aggregate in AD. It easily self-assembles into nanofibers (**Figure 1**). The binding response of NB to FF was tested. To avoid the interference of various FF concentrations, 0.22 mg/ml of FF was kept constant across the whole experiment with varied NB from low to high concentrations. At low concentration (6.2×10^{-5} M of NB), NB was able to recognize and image the self-assembled FF nanofibers via fluorescence imaging (**Figure 1A, 1D, 1G**); while at high concentration (1.0×10^{-3} M), a large number of NB molecules competitively inhibited self-assembly of FF by occupying the self-assembly sites of FF to produce small FF nanophase segments (**Figure 1C, 1F, 1I**).[26] Moreover, NB also self-assembled into flat nano-rods in a concentration-independent manner (**Figure 1J, 1K, 1L**), but simultaneously exhibited inhibitory effect on FF self-assembly in a dose-dependent manner (**Figure 1A-1I**).

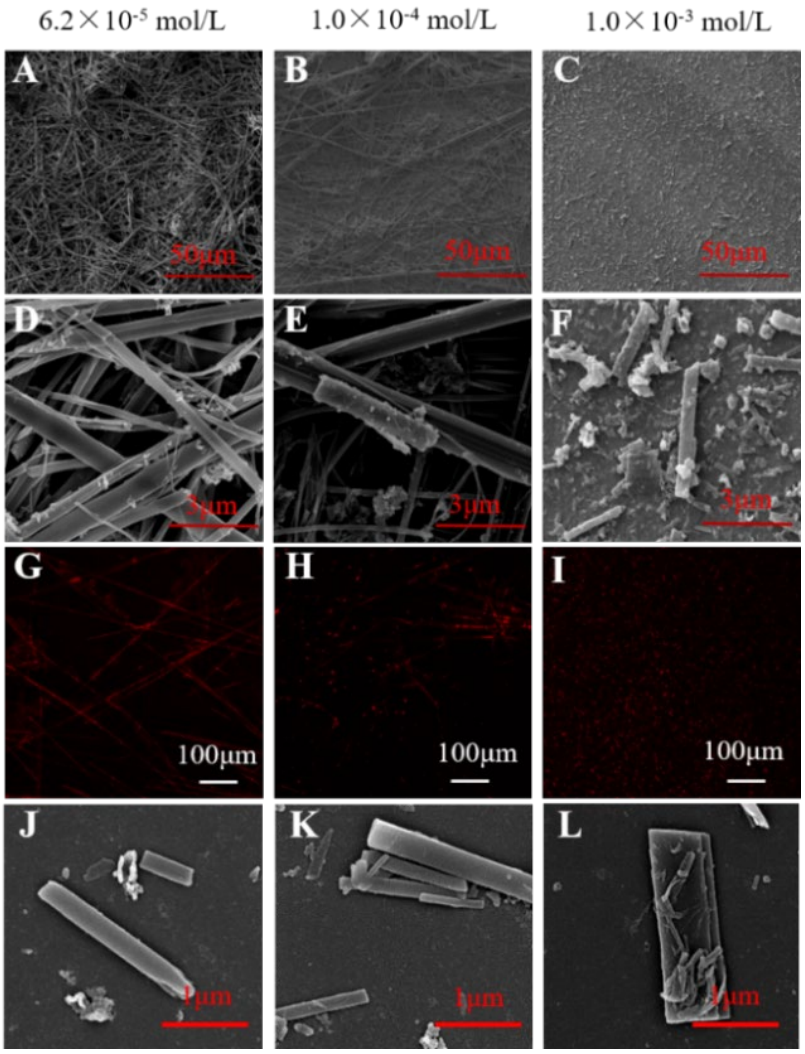

Figure 1. SEM (A-F) and confocal laser fluorescence imaging (G-I) of self-assembly of FF (0.22 mg/ml) with NB at different concentrations, from low to high concentration. SEM (J-L) of self-assembly of NB at different concentrations.

When a variety of truncated fragments of Aβ was analyzed, a remarkable occurrence of aromatic residues was found to be responsible for exacerbating Aβ aggregation.[26-29] The aromatic residues in various fragments raise the possibility that π-π interactions may play a significant role in the molecular recognition of FF at the C-terminus of Aβ fragment that leads to Aβ aggregation.[10, 27] Atomic Force Microscopy (AFM) has been considered a powerful tool in analyzing the interaction forces between two molecules.[17] The interaction force between NB and FF nanofibers or Aβ oligomers was verified by AFM to identify the specific binding of NB to FF (**Figure S2**). Our results clearly demonstrated a significant interaction force of 0.231 nN

between NB and FF nanofibers, which is similar to that between NB and Aβ oligomers (0.230 nN). However, the test substrate, mica, had little-to-no interaction with NB (0.001 nN). Strong adhesion forces between NB and FF nanofibers or Aβ oligomers were observed very frequently in this experiment. NB staining fluorescence imaging was performed through the π-π interaction with FF in Aβ, and NB consequently exerted an inhibitory effect on the aggregation of Aβ. Since the π-junction of Aβ oligomers was occupied by NB, NB competitively inhibited the further aggregation of Aβ oligomers.

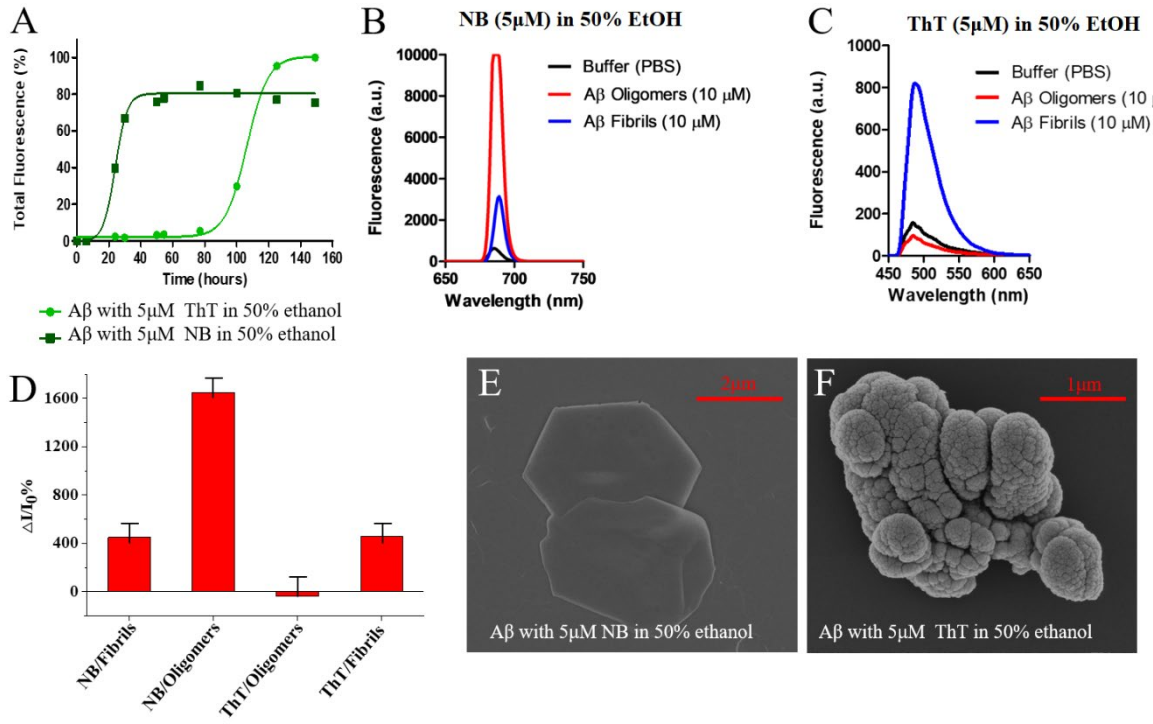

Figure 2. (A) Aβ aggregation assay: *in vitro* study to detect Aβ aggregation over time. ThT was used to detect formation of fibrillar Aβ species. Total fluorescence (%) was plotted as the fluorescence intensity divided by the maximum fluorescence intensity obtained in the plateau; (B) and (C) Fluorescence emission of NB and ThT response to buffer (background fluorescence, black line), oligomer and fibrils; (D) △I refers to the increased fluorescence intensity, I_0 corresponds to the background fluorescence of NB or ThT; Aβ morphology was analyzed by scanning electron microscopy (SEM) after 160 hours of incubation with NB (E) or ThT (F).

As reported previously, monomeric Aβ aggregated into Aβ oligomers within 24 hours,[15] and after 72 hours, the Aβ fibrils could be detected using Thioflavin-T (ThT) in green fluorescence.[30] To monitor the aggregation of Aβ over time, co-incubation of 5μM ThT or 5μM

NB in ethanol/H_2O (1:1, v/v) with Aβ was carried out. After 72 hours, the fluorescence intensity of ThT was slightly increased, indicating the beginning formation of Aβ fibrils **(Figure 2A, ●)**. While the fluorescence intensity of NB was rapidly increased after 10 hours and reached plateau only after 40 hours, suggesting that NB shortened the nucleation phase **(Figure 2A, ■)**. The sharp elevation of binding-induced fluorescence at 24 hours was associated with NB-specific Aβ species. We were not been able to detect the formation of Aβ fibrils at earlier time points by using NB. This data suggests that NB inhibits the transformation of oligomers into fibrils. Furthermore, the capability of NB to distinguish Aβ oligomers from Aβ fibrils was assessed in the solution of Aβ oligomers and fibrils using fluorescence spectrometry.[31] As a result, there was an NB fluorescence increase of 1650%±1% and 450%±10% by Aβ oligomers and Aβ fibrils, respectively, through a selective binding (**Figure 2B**, **2D**). In comparison, ThT fluorescence intensity did not increase with Aβ oligomers but increased 460%±10% with Aβ fibrils (**Figure 2C, 2D**), which was consistent with previous reports in that ThT is a binder of Aβ fibrils.[32] Furthermore, the morphology of Aβ aggregates was analyzed by SEM after initial aggregation of Aβ monomers for 160 hours. We found that Aβ exhibited a hexagonal structure in the presence of NB **(Figure 2E**), whereas, in the presence of ThT, Aβ displayed a complex aggregated structure (**Figure 2F**). This suggests that NB could influence the conformational aggregation of Aβ to keep Aβ's native folding, indicating that NB could inhibit Aβ from aggregating into fibrillar species, but ThT did not show the same effect. To quantify the affinity of NB to Aβ oligomers, the apparent binding constants (K_d and B_{max}) of NB was measured by a saturation binding assay (**Figure 3**). NB exhibited an excellent affinity to Aβ oligomers at an equilibrium dissociation constant (K_d) value of 6.4 nM and maximum binding B_{max} of 10489 a.u.

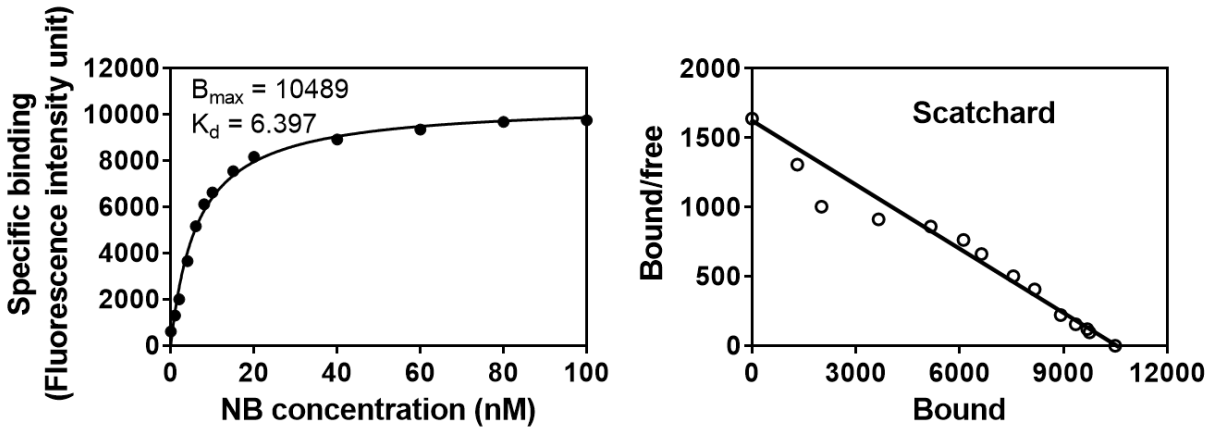

Figure 3. Measurement of the apparent binding constant (K_d and B_{max}) of NB to Aβ oligomers. Plot of the fluorescence intensity (E_x = 591 nm, E_m = 682 nm) as a function of the concentration of NB in the presence of $Aβ_{40}$ oligomers (2 μM).

In the Aβ aggregation process, the core is intertwined into insoluble fibrils, surrounded by a ring-like structure composed of soluble oligomers that may eventually be evolved into fibrils.[33] In Aβ fibrils, a shallow groove is formed by alternating conformers of aromatic rings, stabilized by packing interactions with adjacent residues.[34, 35] The aromatic shallow groove is indispensable for ThS to bind and recognize Aβ fibrils.[32] Previous work demonstrated that the binding ability of ThS to Aβ fibrils would be greatly reduced without this aromatic shallow groove.[36, 37] NB was designed based on the molecular structure of FF in Aβ, allowing its binding to FF through π-π stacking. Next, we determined if NB as a new near infrared fluorescent probe could be used in imaging AD brain for pathological assessment. As shown in **Figure S3,** a distance of 11.4 to 16.2 Å was found in the NB molecule between the benzothiazole-containing donor and acceptor, consistent with previous report.[23] Interestingly, the size of the FF molecule of Aβ is also in this distance range, and the two aromatic rings of FF overlay well with the two aromatic rings of NB, forming a stable π-π stacking; while the carboxyl and amino groups of FF further promoted the NB-FF binding (**Scheme 1B**). The reason for differential staining of Aβ by NB and ThS may lies in the following: (1) The molecular weight of NB is about three times larger than that of ThS; (2) Due to a greater steric hindrance, NB is not able to enter the

shallow groove of the Aβ formed by aromatic ring; (3) The NB binding motif in Aβ is FF. When Aβ form β-folds, the folding point is right at FF to form Aβ oligomers. As illustrated in **Scheme 1**, the FFs in Aβ oligomers were almost completely exposed, as a result, NB recognized and responded to Aβ oligomers robustly.

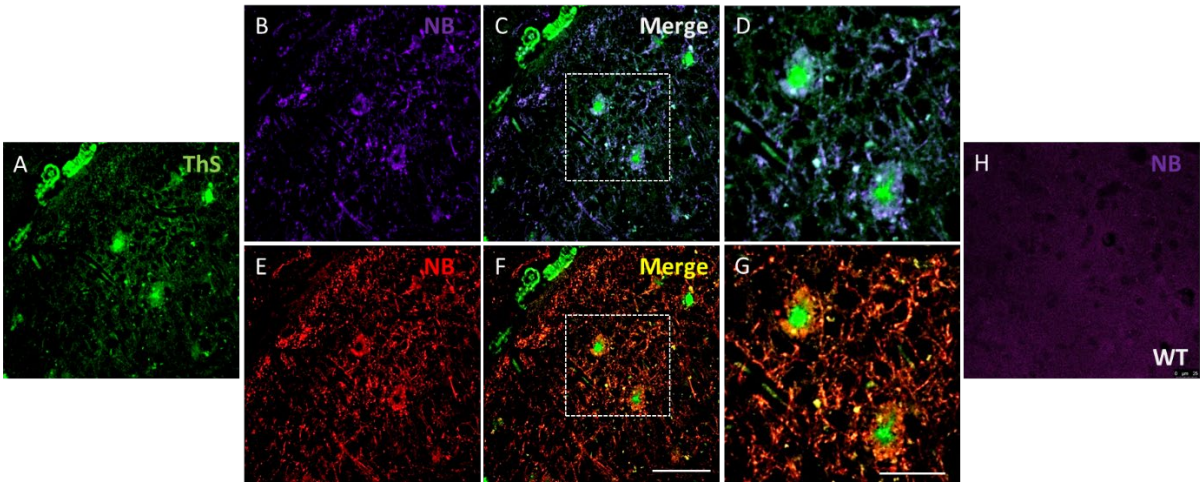

Figure 4. Confocal microphotography of mouse AD hippocampus stained with ThS and NB. A-D) excitation wavelength at 488 nm for ThS (green) and 640 nm for NB (purple), merged in white. A, E-G) excitation wavelength at 488 nm for ThS (green) and 561 nm for NB (red), merged in yellow. D, G) Dotted squares in C and F were zoomed in for higher resolution. H) Microphotography of wild-type hippocampus stained with NB used as control. Scale bar: 50 μm (A-C, E-F, H), 25 μm (D, G).

The hippocampus, involved in learning and memory, is one of the main brain areas affected in AD.[38] To evaluate NB's capability to detect Aβ oligomers in AD brains, sections containing cortical and hippocampal areas were obtained from APP/PSEN1 mice, which overexpresses mutated amyloid precursor protein (APP) and presenilin 1 (PS1).[33, 39, 40] Thioflavin S (ThS) is a universally used fluorescent dye that stains fibrillar amyloid when exited at 435 nm, emitting at 485 nm.[41] ThS/NB double staining of AD mouse brain clearly demonstrated the ThS green fluorescence staining of Aβ fibrils, surrounded by NB red/purple fluorescence staining of Aβ oligomers (**Figure 4**). In addition, wild-type control mice did not show NB staining. To determine the specific wavelength to visualize NB, confocal images of ThS/NB stained brain samples from AD mice were analyzed at 485 nm (green for ThS), and 561 nm (red) or 640 nm (purple) for NB. As shown in **Figure 4**, excitation of the fluorophore at different wavelengths

exhibited similar fluorescence intensity and sensitivity (background/signal ratio), indicating that NB can be easily visualized with either epifluorescence or confocal microscopes, and can also provide a NIR signal that allows for less overlapping with other commonly used dyes.

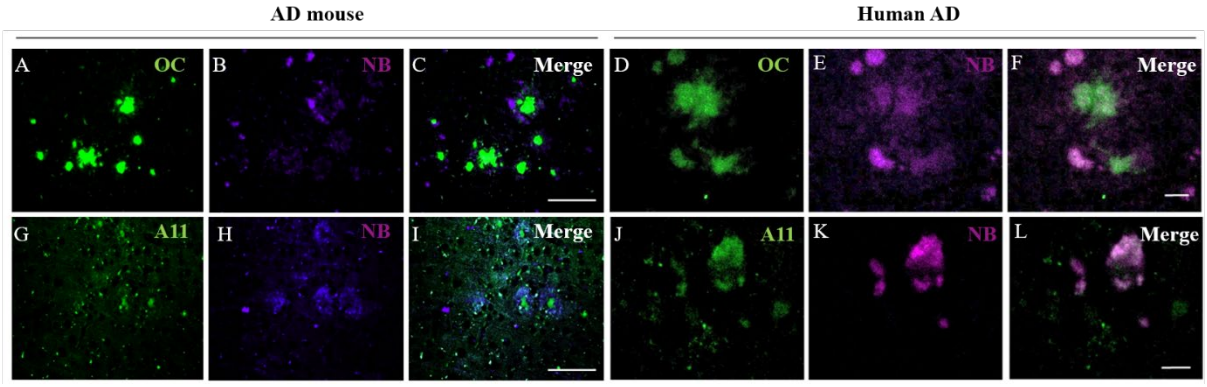

Figure 5. Confocal microscopy of mouse and human Alzheimer's brain using NB staining. Double staining was performed using NB to co-localize with the conformational antibody OC staining for soluble fibrillar Aβ (middle panels), and A11 antibody staining for oligomeric Aβ (bottom panels). Merged images are shown and the co-localization of both staining is shown in white. Scale bar: 50 µm (in mouse panels) and 10 µm (in human panels).

OC and A11 are specific antibodies commercially available to recognize fibrillar oligomers and oligomeric amyloid, respectively.[41-43] Double staining (ThS/NB, OC/NB, A11/NB) of AD mouse and AD human brain samples was performed to evaluate the specificity of NB for Aβ oligomers by confocal microscopy. The co-staining of ThS/NB further demonstrated a ThS-positive staining in the core of mature plaques in green, while NB stained Aβ in the periphery of the core in purple surrounding ThS green fluorescence (**Figure 5A-C**). In human brain, it seems the NB staining colocalized more with ThS staining, compared to the co-staining in mouse brains (**Figure 5D-F**). OC antibody recognizes fibrillar oligomers, but not natively folded Aβ. Double staining with NB and OC barely overlapped in mouse samples (**Figure 5G-I**) but partially colocalized in human tissue (**Figure 5J-L**), confirming that NB recognizes Aβ oligomers. In A11/NB double staining, the NB-positive area was highly overlapped with A11 staining both in mouse (**Figure 5M-O**) and human samples (**Figure 5P-**

R), ratifying that NB is able to recognize oligomeric Aβ. The variations obtained in the staining of Aβ aggregates in mouse and human samples, may partially be caused by the variations of experimental conditions between the two studies, e.g. the different protocols for tissue processing as well as the staining including the solvents used across the experiments. Also, the compositions of Aβ species may be different between specimens. Human Aβ aggregates are more diverse, containing Aβ conformations of different nature.[44] Nevertheless, further validation of this result, especially by examining more human specimen will help to better understand the discrepancy. In conclusion, NB staining overlapped with A11 (oligomeric Aβ), partially colocalized with OC (fibrillar oligomeric Aβ) and ThS (fibrillar Aβ) in human, and barely overlapped with OC (fibrillar oligomeric Aβ) in mouse samples. This indicates that NB is a promising fluorescent probe to mainly detect several types of oligomeric Aβ species, an early pathological event at the early stage of AD.

Since the NB has two outstanding properties: (1) it shows robust response to oligomeric Aβ upon specific binding with remarkably increased fluorescence intensity (1650%), hence this property may lead to further development of the NB probe into a novel *in vivo* imaging modality for AD patients in early diagnosis. Towards this goal, an actionable program may include the following investigations in animal models: (a) the development of a NB probe delivery system targeting the brain, (b) the test of the NB probe to determine the fluorescence intensity in the *in vivo* imaging system and (c) the improvement of the probe to maximize its capability in *in vivo* imaging. (2) The NB probe demonstrates superior inhibitory effect on Aβ aggregation and fibril formation; hence, this could lead to the development of a novel drug for AD patients. To reach this goal, a preclinical study of NB in animal models of AD will be performed, to determine the efficacy of NB in blocking Aβ aggregation and fibril formation in aged AD animals (e.g. APP/PS1 mice) and in ameliorating AD disease and dementia. Alternatively, an analogue of NB may be developed as a potent drug for AD patients. Nevertheless, all these preclinical

studies are warranted for future translational studies and clinical trials to assess the clinical value of NB.

Supporting Information

Supporting Information is available from the Wiley Online Library or from the author.

Acknowledgements

This work was supported by grants from the start-up fund of Huaiyin Institute of Technology, the Natural Science Foundation of Jiangsu Provincial Department of Education (17KJB530001), the Natural Science Foundation of China (51803068 and 31470926), Jiangsu Government Overseas Studies Scholarship (JS-2017-201), the International Cooperation in Science and Technology Research projects (HAC201615), Jiangsu Qing Lan project, and the Brain and Behavior Research Foundation 27565 2018 NARSAD, PID2019-107090RA-I00 Spanish Ministry of Science, Innovation and Universities, and Ramony Cajal Program RYC-2017-21879 to IM-G. Thanks for the support Atomic Force Microscopy (AFM)/Scanning Electron Microscopy (SEM) Core of Houston Methodist Hospital Research Institute.

Author contributions

The initial discovery and application of BODIPY in the diagnosis of Alzheimer's disease was made by L.Q. The experimental design and data analysis were performed by L.Q., T.W., I.M.G. and Z.G.X.. The experimental laboratory work was performed by Q.Y.S., W.H.L., N.G., J.H.G., L.V.G. and R.G.G.. L.Q., T.W., I.M.G., Z.G.X. were primary writers of the manuscript. L.Q. and T.F.W. were the principal investigators to oversee the entire study. All authors discussed the results and provided feedback on the manuscript.

Conflict of Interest

The authors declare no conflict of interest.

Received: ((will be filled in by the editorial staff))

Revised: ((will be filled in by the editorial staff))

Published online: ((will be filled in by the editorial staff))

References

[1] Zhao Y, Cai J, Liu Z, Li Y, Zheng C, Zheng Y, et al. Nanocomposites Inhibit the Formation, Mitigate the Neurotoxicity, and Facilitate the Removal of beta-Amyloid Aggregates in Alzheimer's Disease Mice. *Nano letters*. 2019;19:674-83.
[2] Rakez Kayed EH, Jennifer L. Thompson, Theresa M. McIntire, Saskia C. Milton, Carl W. Cotman, Charles G. Glabe. Common Structure of Soluble Amyloid Oligomers Implies Common Mechanism of Pathogenesis. *Science*. 2003:486-9.
[3] Li T, Braunstein KE, Zhang J, Lau A, Sibener L, Deeble C, et al. The neuritic plaque facilitates pathological conversion of tau in an Alzheimer's disease mouse model. *Nature communications*. 2016;7:12082.
[4] Tolar M, Abushakra S, Sabbagh M. The path forward in Alzheimer's disease therapeutics: Reevaluating the amyloid cascade hypothesis. *Alzheimer's & Dementia*. 2020;16:1553-60.
[5] Hey JA, Yu JY, Versavel M, Abushakra S, Kocis P, Power A, et al. Clinical Pharmacokinetics and Safety of ALZ-801, a Novel Prodrug of Tramiprosate in Development for the Treatment of Alzheimer's Disease. *Clin Pharmacokinet*. 2018;57:315-33.
[6] Frydman-Marom A, Rechter M, Shefler I, Bram Y, Shalev DE, Gazit E. Cognitive-performance recovery of Alzheimer's disease model mice by modulation of early soluble amyloidal assemblies. *Angew Chem Int Ed Engl*. 2009;48:1981-6.
[7] Jakob-Roetne R, Jacobsen H. Alzheimer's disease: from pathology to therapeutic approaches. *Angew Chem Int Ed Engl*. 2009;48:3030-59.
[8] Mohanrao R, Sureshan KM. Synthesis and Reversible Hydration of a Pseudoprotein, a Fully Organic Polymeric Desiccant by Multiple Single-Crystal-to-Single-Crystal Transformations. *Angew Chem Int Ed Engl*. 2018;57:12435-9.
[9] Yakupova EI, Bobyleva LG, Vikhlyantsev IM, Bobylev AG. Congo Red and amyloids: history and relationship. *Biosci Rep*. 2019;39.
[10] Wang D, Deng J, Deng X, Fang C, Zhang X, Yang P. Controlling Enamel Remineralization by Amyloid-Like Amelogenin Mimics. *Advanced materials*. 2020;32:e2002080.
[11] Kim D, Kwon HJ, Hyeon T. Magnetite/Ceria Nanoparticle Assemblies for Extracorporeal Cleansing of Amyloid-beta in Alzheimer's Disease. *Advanced materials*. 2019;31:e1807965.
[12] Yao Y, Nzou G, Alle T, Tsering W, Maimaiti S, Trojanowski JQ, et al. Correction of microtubule defects within Abeta plaque-associated dystrophic axons results in lowered Abeta release and plaque deposition. *Alzheimers Dement*. 2020;16:1345-57.
[13] Hintersteiner M, Enz A, Frey P, Jaton AL, Kinzy W, Kneuer R, et al. In vivo detection of amyloid-beta deposits by near-infrared imaging using an oxazine-derivative probe. *Nat Biotechnol*. 2005;23:577-83.
[14] Chen GF, Xu TH, Yan Y, Zhou YR, Jiang Y, Melcher K, et al. Amyloid beta: structure, biology and structure-based therapeutic development. *Acta Pharmacol Sin*. 2017;38:1205-35.
[15] Dahlgren KN, Manelli AM, Stine WB, Jr., Baker LK, Krafft GA, LaDu MJ. Oligomeric and fibrillar species of amyloid-beta peptides differentially affect neuronal viability. *J Biol Chem*. 2002;277:32046-53.
[16] Gorbitz CH. The structure of nanotubes formed by diphenylalanine, the core recognition motif of Alzheimer's beta-amyloid polypeptide. *Chem Commun (Camb)*. 2006:2332-4.
[17] Quan L, Gu J, Lin W, Wei Y, Lin Y, Liu L, et al. A BODIPY biosensor to detect and drive self-assembly of diphenylalanine. *Chem Commun (Camb)*. 2019.
[18] Nakamura A, Kaneko N, Villemagne VL, Kato T, Doecke J, Doré V, et al. High performance plasma amyloid-β biomarkers for Alzheimer's disease. *Nature*. 2018;554:249-54.
[19] Cespedes MV, Cano-Garrido O, Alamo P, Sala R, Gallardo A, Serna N, et al. Engineering Secretory Amyloids for Remote and Highly Selective Destruction of Metastatic Foci. *Advanced materials*. 2020;32:e1907348.

[20] Thomas J. Grabowski HSC, Jean Paul G. Vonsattel, and Steven M. Greenberg. Novel Amyloid Precursor Protein Mutation in an Iowa Family with Dementia and Severe Cerebral Amyloid Angiopathy. *Annals of Neurology*. 2001;49:697-705.
[21] Gu L, Liu C, Stroud JC, Ngo S, Jiang L, Guo Z. Antiparallel triple-strand architecture for prefibrillar Abeta42 oligomers. *J Biol Chem*. 2014;289:27300-13.
[22] Lee S, Fernandez EJ, Good TA. Role of aggregation conditions in structure, stability, and toxicity of intermediates in the Abeta fibril formation pathway. *Protein Sci*. 2007;16:723-32.
[23] Verwilst P, Kim HR, Seo J, Sohn NW, Cha SY, Kim Y, et al. Rational Design of in Vivo Tau Tangle-Selective Near-Infrared Fluorophores: Expanding the BODIPY Universe. *Journal of the American Chemical Society*. 2017;139:13393-403.
[24] Asem H, Zhao Y, Ye F, Barrefelt A, Abedi-Valugerdi M, El-Sayed R, et al. Biodistribution of biodegradable polymeric nano-carriers loaded with busulphan and designed for multimodal imaging. *J Nanobiotechnology*. 2016;14:82.
[25] Wang X, Liu D, Huang HZ, Wang ZH, Hou TY, Yang X, et al. A Novel MicroRNA-124/PTPN1 Signal Pathway Mediates Synaptic and Memory Deficits in Alzheimer's Disease. *Biol Psychiatry*. 2018;83:395-405.
[26] Levy M, Garmy N, Gazit E, Fantini J. The minimal amyloid-forming fragment of the islet amyloid polypeptide is a glycolipid-binding domain. *The FEBS journal*. 2006;273:5724-35.
[27] Gazit E. A possible role for pi-stacking in the self-assembly of amyloid fibrils. *FASEB J*. 2002;16:77-83.
[28] Shaham-Niv S, Rehak P, Vuković L, Adler-Abramovich L, Král P, Gazit E. Formation of Apoptosis-Inducing Amyloid Fibrils by Tryptophan. *Israel Journal of Chemistry*. 2017;57:729-37.
[29] Azriel R, Gazit E. Analysis of the minimal amyloid-forming fragment of the islet amyloid polypeptide. An experimental support for the key role of the phenylalanine residue in amyloid formation. *J Biol Chem*. 2001;276:34156-61.
[30] Naiki H, Okoshi T, Ozawa D, Yamaguchi I, Hasegawa K. Molecular pathogenesis of human amyloidosis: Lessons from beta2 -microglobulin-related amyloidosis. *Pathol Int*. 2016;66:193-201.
[31] Hoshi M, Sato M, Matsumoto S, Noguchi A, Yasutake K, Yoshida N, et al. Spherical aggregates of beta-amyloid (amylospheroid) show high neurotoxicity and activate tau protein kinase I/glycogen synthase kinase-3beta. *Proc Natl Acad Sci U S A*. 2003;100:6370-5.
[32] Biancalana M, Koide S. Molecular mechanism of Thioflavin-T binding to amyloid fibrils. *Biochim Biophys Acta*. 2010;1804:1405-12.
[33] Ecroyd H, Carver JA. Unraveling the mysteries of protein folding and misfolding. *IUBMB Life*. 2008;60:769-74.
[34] Chun Wu ZW, Hongxing Lei, Wei Zhang, and Yong Duan*. Dual binding modes of Congo red to amyloid protofibril surface observed in molecular dynamics simulations.pdf. *J AM CHEM SOC*. 2007;129:1225-32.
[35] Wu C, Biancalana M, Koide S, Shea JE. Binding modes of Thioflavin-T to the single-layer beta-sheet of the peptide self-assembly mimics. *Journal of molecular biology*. 2009;394:627-33.
[36] Sabate R, Lascu I, Saupe SJ. On the binding of Thioflavin-T to HET-s amyloid fibrils assembled at pH 2. *Journal of structural biology*. 2008;162:387-96.
[37] Ritu Khurana CI-Z, y Maighdlin Pope,y Jie Li,* Liza Nielson,* Marina Ramı´rez-Alvarado,z Lynn Regan,z Anthony L. Fink,* and Sue A. Cartery. A general model for amyloid fibril assembly based on morphological studies using atomic force microscopy, Biophys.pdf. *Biophysical Journal* 2003; 85:1135–44.
[38] Bienkowski MS, Bowman I, Song MY, Gou L, Ard T, Cotter K, et al. Integration of gene expression and brain-wide connectivity reveals the multiscale organization of mouse hippocampal networks. *Nature neuroscience*. 2018;21:1628-43.
[39] Haass C, Selkoe DJ. Soluble protein oligomers in neurodegeneration: lessons from the Alzheimer's amyloid beta-peptide. *Nat Rev Mol Cell Biol*. 2007;8:101-12.
[40] Dietmar R. Thal MUR, MD; Mario Orantes, MD; and Heiko Braak, MD. Phases of A □-deposition in the human brain and its relevance for the development of AD. *Neurology*. 2002;58:1791‑800.
[41] Lord A, Kalimo H, Eckman C, Zhang XQ, Lannfelt L, Nilsson LN. The Arctic Alzheimer mutation facilitates early intraneuronal Abeta aggregation and senile plaque formation in transgenic mice. *Neurobiology of aging*. 2006;27:67-77.
[42] Venkataramani V, Wirths O, Budka H, Hartig W, Kovacs GG, Bayer TA. Antibody 9D5 recognizes oligomeric pyroglutamate amyloid-beta in a fraction of amyloid-beta deposits in Alzheimer's disease without cross-reactivity with other protein aggregates. *J Alzheimers Dis*. 2012;29:361-71.
[43] Kim HJ, Ajit D, Peterson TS, Wang Y, Camden JM, Gibson Wood W, et al. Nucleotides released from Abeta(1)(-)(4)(2) -treated microglial cells increase cell migration and Abeta(1)(-)(4)(2) uptake through P2Y(2) receptor activation. *J Neurochem*. 2012;121:228-38.
[44] Duran-Aniotz C, Moreno-Gonzalez I, Gamez N, Perez-Urrutia N, Vegas-Gomez L, Soto C, et al. Amyloid pathology arrangements in Alzheimer's disease brains modulate in vivo seeding capability. *Acta Neuropathol Commun*. 2021;9:56.

TOC

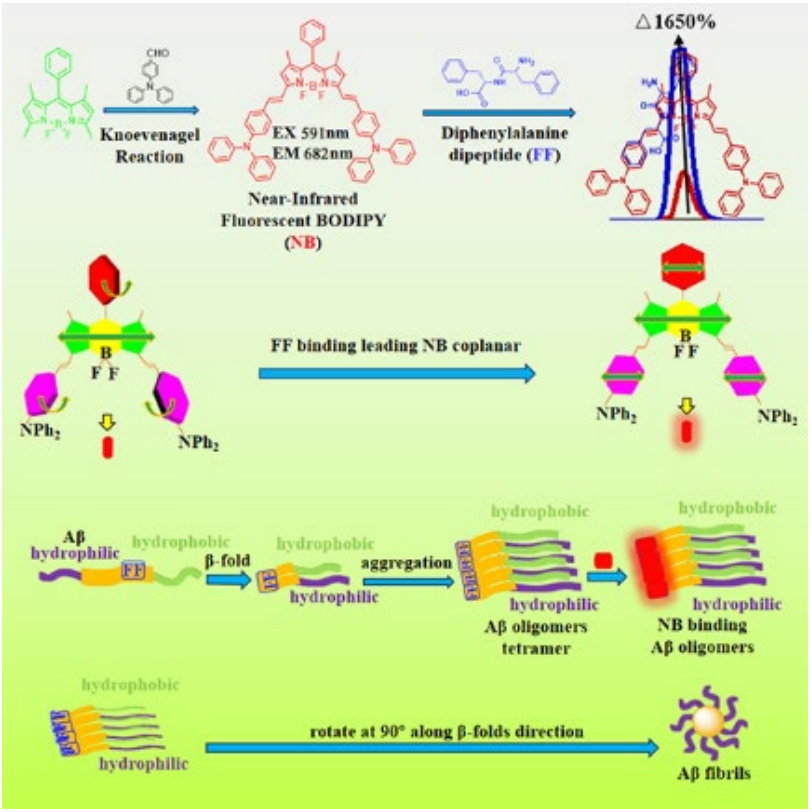
△1650%
Knoevenagel Reaction
EX 591nm
EM 682nm
Near-Infrared Fluorescent BODIPY (NB)
Diphenylalanine dipeptide (FF)
FF binding leading NB coplanar
Aβ hydrophilic
hydrophobic
FF
β-fold
hydrophobic
hydrophilic
aggregation
hydrophobic
hydrophilic
Aβ oligomers tetramer
hydrophobic
hydrophilic
NB binding Aβ oligomers
hydrophobic
hydrophilic
rotate at 90° along β-folds direction
Aβ fibrils

Supporting Information

A near-infrared probe for detecting and interposing amyloid beta oligomerization in early Alzheimer's disease

Li Quan,[1,2]* Ines Moreno-Gonzalez,[3,6]* Zhigang Xie[4]* Nazaret Gamez,[3,6] Qinyong Song,[1] Jianhua Gu,[5] Laura Vegas-Gomez,[6] Wenhai Lin,[4] Ruben Gomez-Gutierrez,[3] Tianfu Wu[2]*

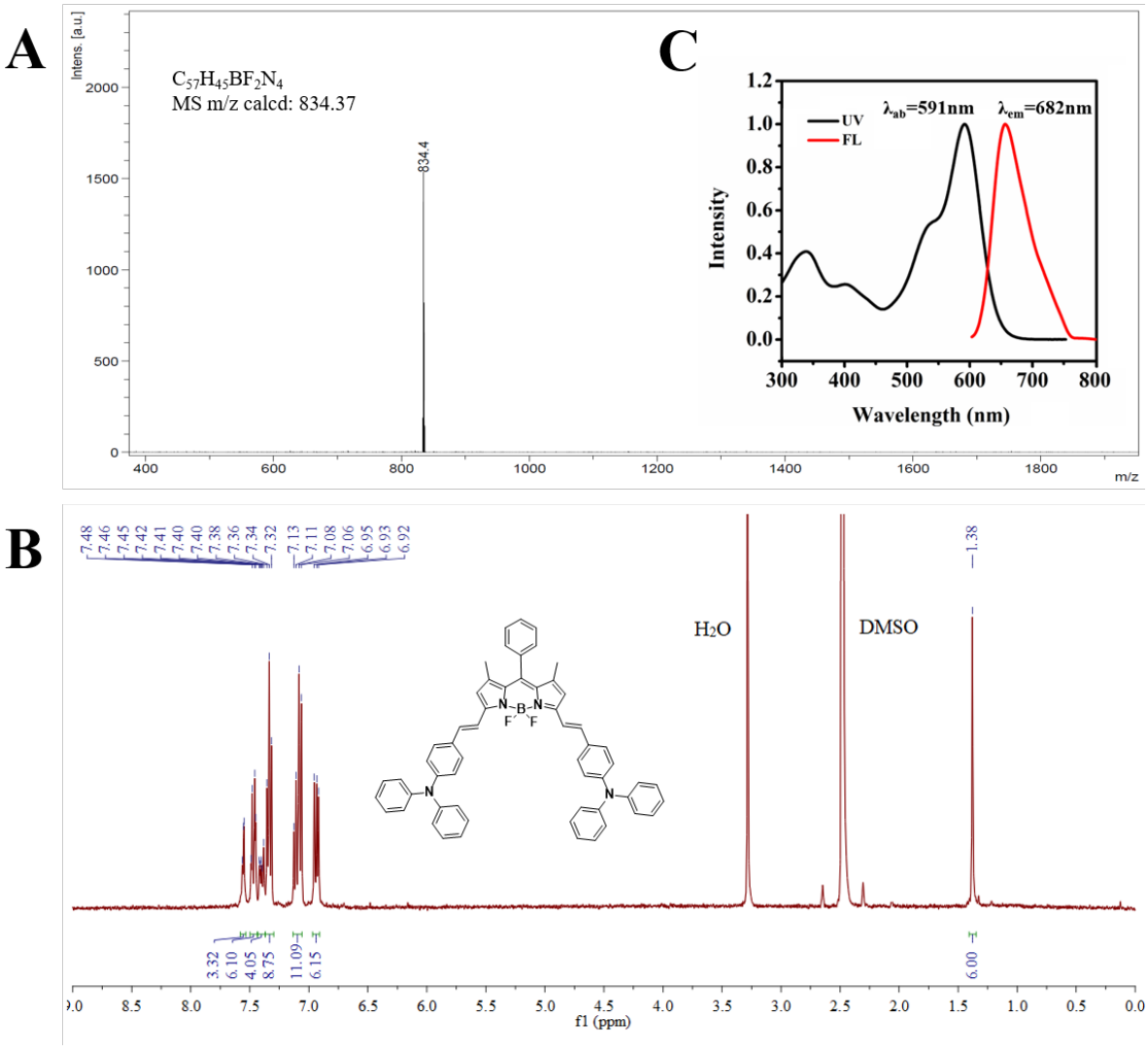

Figure S1. Character of NB. A) MS; B) ^{1}H NMR; C) UV absorption and FL emission of NB.

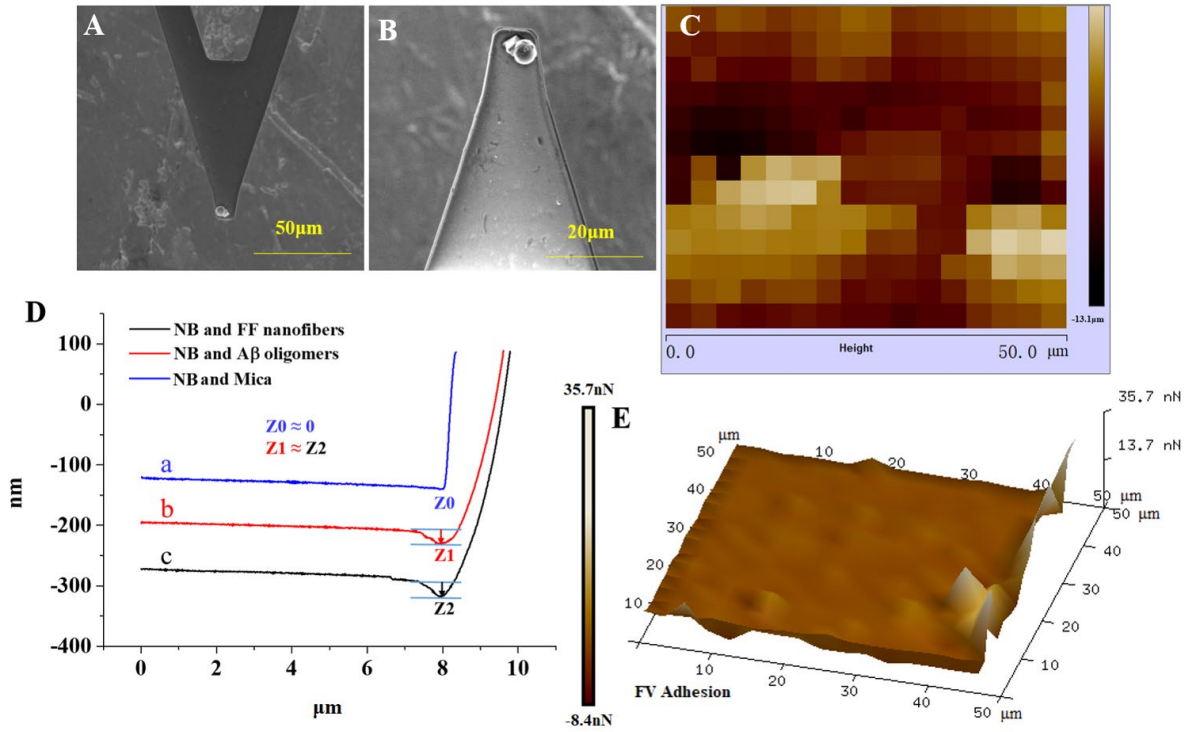

Figure S2. (A, B) SEM image of the NB-modified beaded tip, (C) height and (E) adhesion maps of NB binding events on Aβ oligomers with AFM, and (D) adhesion forces between NB and Mica (a, 0.001nN), or Aβ oligomers (b, 0.230nN), or FF nanofibers (c, 0.231nN). F = K·Z, F stands for atomic force; K = 0.01N/M; Z stands for the distance between Baseline and peak valley.

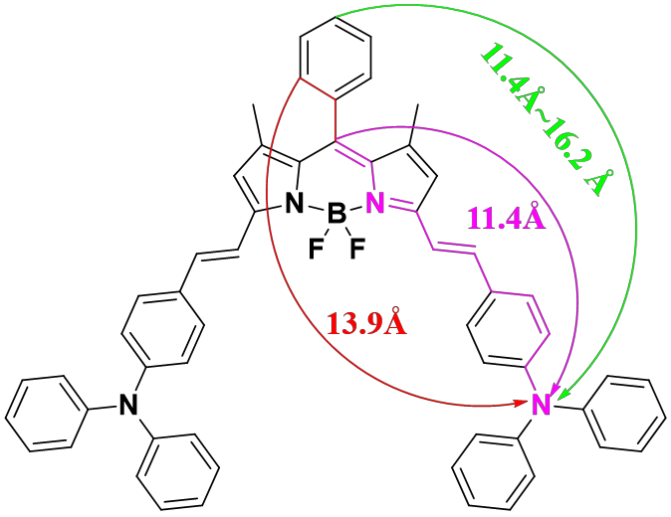

Figure S3. NB has similar units of compounds reported in the literature with the distance of 11.4 to 16.2 Å of benzothiazole-containing donor acceptor.